Qian, J., Zhang, L., **Schlink, U.**, Meng, Q., Liu, X., Janscó, T. (2024):
High spatial and temporal resolution multi-source anthropogenic heat estimation for China
Resour. Conserv. Recycl. **203** , art. 107451

https://doi.org/10.1016/j.resconrec.2024.107451

High spatial and temporal resolution multi-source anthropogenic heat estimation for China

Jiangkang Qian[a,b,d], *Linlin Zhang*[a,b,c,*], *Uwe Schlink*[d], *Qingyan Meng*[a,b,c], *Xue Liu*[e], *Tamás Jancsó*[f]

a. Aerospace Information Research Institute, Chinese Academy of Sciences, Beijing, 100094, China
b. University of Chinese Academy of Sciences, Beijing, 100049, China
c. Key Laboratory of Earth Observation of Hainan Province, Hainan Aerospace Information Research Institute, Sanya, 572029, China
d. Department of Urban and Environmental Sociology, Helmholtz Centre for Environmental Research-UFZ, Leipzig, D-04318, Germany
e. School of Geographic Sciences, Key Laboratory of Geographic Information Science (Ministry of Education), East China Normal University, Shanghai 200241, China
f. Alba Regia Technical Faculty, Obuda University, Budai ut 45, 8001 Szekesfehervar, Hungary

*Corresponding author: Linlin Zhang
E-mail addresses: zhangll@aircas.ac.cn

Abstract

Anthropogenic heat (AH) emissions have rapidly increased in recent decades and are now critical for studying urban thermal environments; however, datasets of multi-source AH with fine and accurate spatiotemporal characteristics at large scales are lacking. This study advances the top-down inventory method in China with a more rational use of official energy consumption data. Furthermore, we considered features such as the national building height raster, weighted factory density, and weighted road density to better represent the spatial characteristics of multi-source AH. Based on the above, the machine-learning modeling process for AH emissions was optimized using a stacking framework. The results were quantitatively validated using urban climate simulations. This study obtained annual, monthly, and hourly AH of multiple heat sources in China for 2019 at 500 m resolution. The resulting data showed a reasonable AH composition and the total amount and composition of AH varied notably from region to region. The spatial and temporal characteristics of the AH from different sources differed greatly and were more detailed and accurate than those reported in previous studies. Air temperature simulations utilizing this AH dataset were improved. Because of its large spatial extent and detailed spatiotemporal characteristics, the new dataset strongly supports urban climate research and sustainable development.

Keywords: Anthropogenic heat, Machine learning, Model improvement, Spatiotemporal heterogeneity

1. Introduction

Rapid urbanization around the world over the last few decades has been accompanied by an increased population and economic activities (Han et al., 2022; Yang et al., 2022). Urban areas contain more than half of the global population and consume approximately 70% of the energy, which is accompanied by the massive release of anthropogenic heat (AH), which contributes to environmental and demographic problems (Firozjaei et al., 2020; Vargo et al., 2020; Wang et al., 2022a). Despite its negligible contribution to the global energy system, the impact of AH cannot be neglected in major urban built-up areas, where it is almost equal in magnitude to the average daily solar radiation (Hamilton et al., 2009; Iamarino et al., 2012; Sun et al., 2018). The intensity of AH, expressed as heat flux (heat emissions per unit time and area), rapidly increases with growing global energy consumption (Ferreira et al., 2011; Jin et al., 2020). Therefore, AH is a vital component of the urban surface energy balance, which significantly affects the local urban climate and exacerbates the urban heat island effect (Hertel and Schlink, 2022; Qian et al., 2023; Wang et al., 2023). Recognizing the significance of AH emissions in climate simulations, heat-driving patterns, ecological assessments, and sustainable development studies and analyzing their spatial and temporal characteristics have theoretical and practical implications (Dong et al., 2017; Molnar et al., 2020; Wu et al., 2023a).

However, AH at sufficient spatial and temporal resolutions is difficult to obtain via measurements, which hinders further understanding of the urban thermal environment (Qian et al., 2023). For this reason, many AH estimation methods have been proposed to address research requirements at multiple spatial and temporal scales. Current approaches for AH estimation are based on (a) energy consumption inventories, (b) surface energy balance residual methods, and (c) building energy simulations (Grimmond, 1992; Sailor, 2011). Building energy simulations obtain accurate building heat emissions based on building geographic information and typical architectural parameters but cannot be applied in large-scale studies (Alhazmi et al., 2022; Chen et al., 2022b; Vahmani et al., 2022). The traditional surface energy balance method is based on micrometeorological observations, such as eddy flux towers, which attribute the residual term in the energy balance equation to the AH (Offerle et al., 2005; Pigeon et al., 2007). The development and application of remote sensing allow the size of the considered region to be extended (Kato and Yamaguchi, 2005) and new indices have been developed to characterize the effect of AH on urban heat islands (Firozjaei et al., 2020; Wu et al., 2023a); however, uncertainties exist because of unconsidered heat storage and shadows. Although remedies have been proposed (Meng et al., 2023; Yu et al., 2021b), such approaches remain inapplicable to large-scale and multi-temporal AH estimations because of the limited availability of remote sensing data.

The energy consumption inventory method is the most widely used method for AH estimation (Kotthaus and Grimmond, 2012). This method assumes that all AH from energy consumption is dissipated as sensible heat with no hysteresis and can be divided into top-down and bottom-up approaches, depending on the scale variation (Quah and Roth, 2012; Sailor and Lu, 2004). The bottom-up approach relies significantly on detailed geographic information data, statistical data, and parameters of heating and cooling loads (Iamarino et al., 2012; Xu et al., 2021; Zhang et al., 2020). In contrast, the top-down approach is based on large-scale energy consumption data and is more applicable at the global scale or for regions with limited data availability and quality; however, the results are coarser (Allen et al., 2011; Flanner, 2009; Jin et al., 2019). In particular, top-down methods for China tend to use energy consumption data from local statistical yearbooks (Ming et al., 2022; Wang et al., 2019; Yu et al., 2021a); however, unreasonable understanding and use of this data will lead to erroneous estimates of AH (National Bureau of Statistics of China, 2020). In addition to the single methods, AH estimation using combined methods has been increasingly used to solve challenges in complex scenarios (Chow et al., 2014; Meng et al., 2023; Wang et al., 2022a; Zheng and Weng, 2018). However, further details on the associations and distinctions between the different methods are required to realize a more scientific multi-method integration.

Owing to the frequent application of top-down inventory approaches in recent years, many new and improved methods have been proposed. The downscaling of AH based on its association with nighttime light emissions and human activities has been widely implemented (He et al., 2020; Varquez et al., 2021; Wang et al., 2022c). While this method provides a convenient way to obtain large-scale AH, it is biased and unable to capture the complex spatial and temporal characteristics of multi-source AH. New data and methods provide new opportunities for AH modeling. Owing to the development of communication and network technologies, location semantics, spatial interaction, and real-time dynamic information have been applied; however, higher data requirements and tedious workflow limit them to small-scale AH studies (Liu et al., 2021; Ming et al., 2022; Xu et al., 2021). Machine learning can greatly simplify the application of multi-source data and improve the efficiency and accuracy of AH estimation and has gradually become a hot topic in the field of urban thermal environments (Chen et al., 2020; Kim et al., 2022; Qian et al., 2023; Wang et al., 2022d). However, further improvements are required for the refinement of spatiotemporal characteristics, algorithm optimization, and modeling processes (Qian et al., 2022). In summary, bias was present in previous AH datasets because the information contained in the input data was inadequate, the AH was modeled without distinguishing between specific AH sources, or the machine learning models selected were not appropriate.

The validation of these results is another issue in AH studies that is difficult to address. Except for a few studies (Chow et al., 2014; Pigeon et al., 2007) that conducted small-scale field validation based on flux observation towers, most extant studies were limited to qualitative validation by comparing with previous estimates owing to equipment limitations, which is not sufficiently rigorous (Meng et al., 2023). Given these issues, this study proposes an improved

AH estimation method, including the correction of the top-down energy inventory method for China, models based on improved training features, a stacking framework incorporating multiple machine learning algorithms, and validation based on regional climate simulations. This study aims to achieve 1) more accurate estimates of AH values across China in 2019, 2) more reasonable and detailed temporal and spatial variation characteristics of AH from multiple sources, and 3) more scientific and rigorous AH validation.

2. Study area and dataset

Since the late 1970s, China has experienced rapid economic development and urbanization (Yang et al., 2019), resulting in a significant increase in energy consumption and enhanced AH. Strong AH changes the energy fluxes of urban ecosystems and affects the regional climate and atmospheric environment of urban areas, causing frequent extreme heat events, deteriorating air quality, and seriously affecting the health of residents in Chinese cities (Cong et al., 2022; Peng et al., 2021). Therefore, there is an urgent need to clarify the spatial and temporal patterns of AH on a national scale (**Fig. 1**) to explore feasible mitigation measures.

The energy consumption and socioeconomic data for 2019 from the Statistical Yearbooks of Chinese Provinces and Cities (http://www.stats.gov.cn) were used in the energy consumption inventory method. The data involved in the machine learning sample features included Chinese point-of-interest (POI) data from Amap (https://lbs.amap.com), Chinese road and railroad data from open street map (https://www.openstreetmap.org), Chinese building height for 2020 (Wu et al., 2023b), NPP/VIIRS night lighting data (Wu et al., 2023b), MOD11A1 daytime and nighttime land surface temperature (LST), MOD13A1 normalized difference vegetation index (NDVI), NASA global digital elevation model (DEM) data (NASA JPL, 2020), and FLDAS Noah land surface model (Amy et al., 2018) data for air temperature, wind speed, and humidity. In addition, population heat data based on the location information of cell phone users from the Baidu Huiyan big data platform (https://huiyan.baidu.com) were included to describe the dynamic changes in human activities within cities. Additional information on the data is presented in the Supplementary Material.

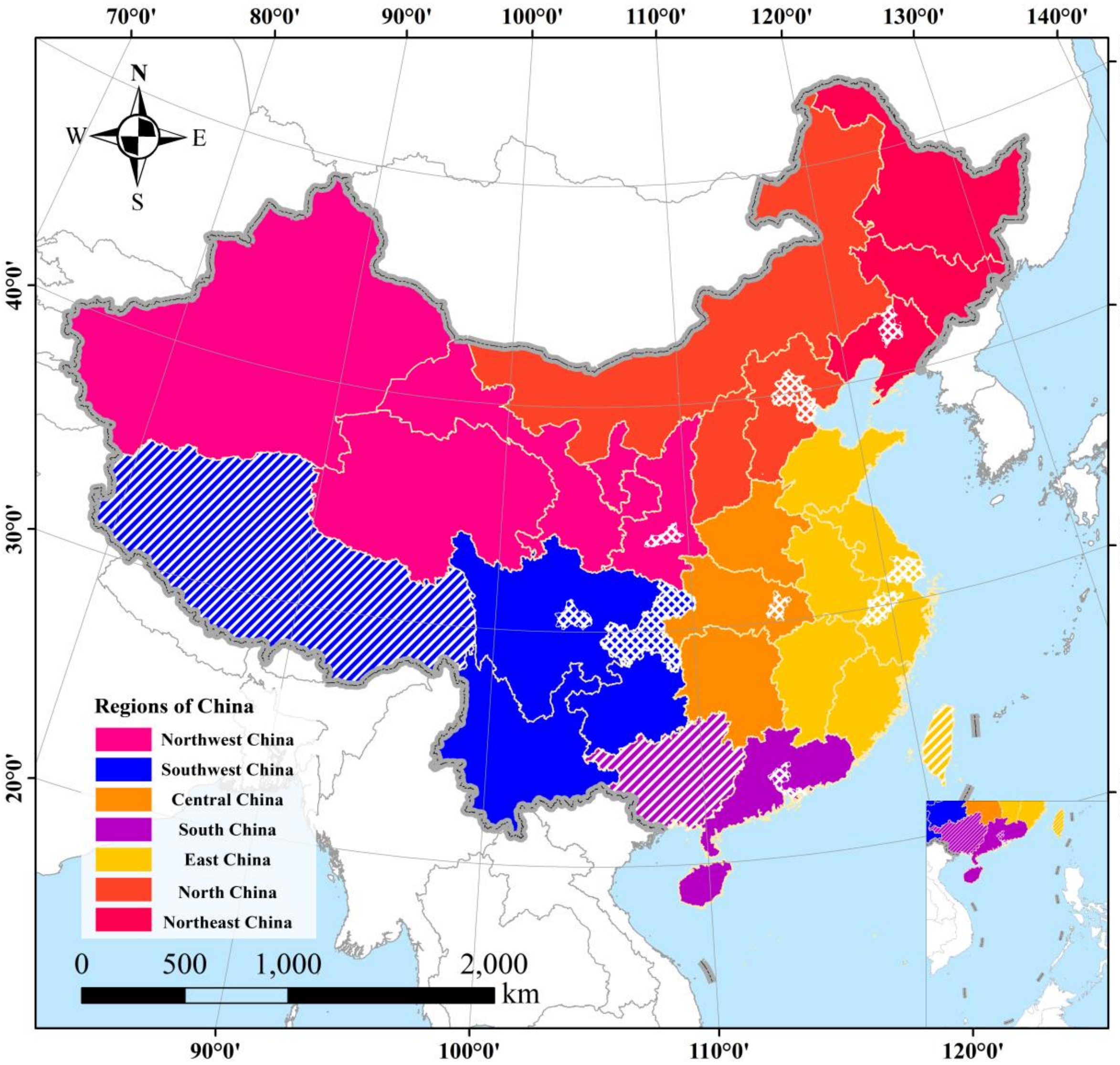

Fig. 1. Study area map. Diagonal slashes indicate regions where statistical data are not available. The diagonal grid coverage indicates the 12 cities where the AH sample is detailed at the district (county) level. The different colors indicate the specific division of the regional calculations involved in this study.

Note: The administrative levels of China involved in this study, from highest to lowest, are provinces, cities, and districts (counties); the lower administrative levels are subordinate to and governed by high levels.

3. Methods

The AH estimation method consisted of sample label estimation, sample feature processing, model construction, and validation of the results (**Fig. 2**). The sample labels in this study represent the AH values to be estimated and the sample features are a set of variables that characterize the properties of the samples. The corrected top-down approach was used to estimate the AH values of the administrative areas as labels. The improved sample features of different AH sources were processed. The samples were then input into a stacking framework containing four machine-learning algorithms and the model was trained. The monthly gridded AH was outputted based on the stacking model and raw data and an hourly AH was derived. Finally, the accuracy of the meteorological simulation was utilized to validate the AH results.

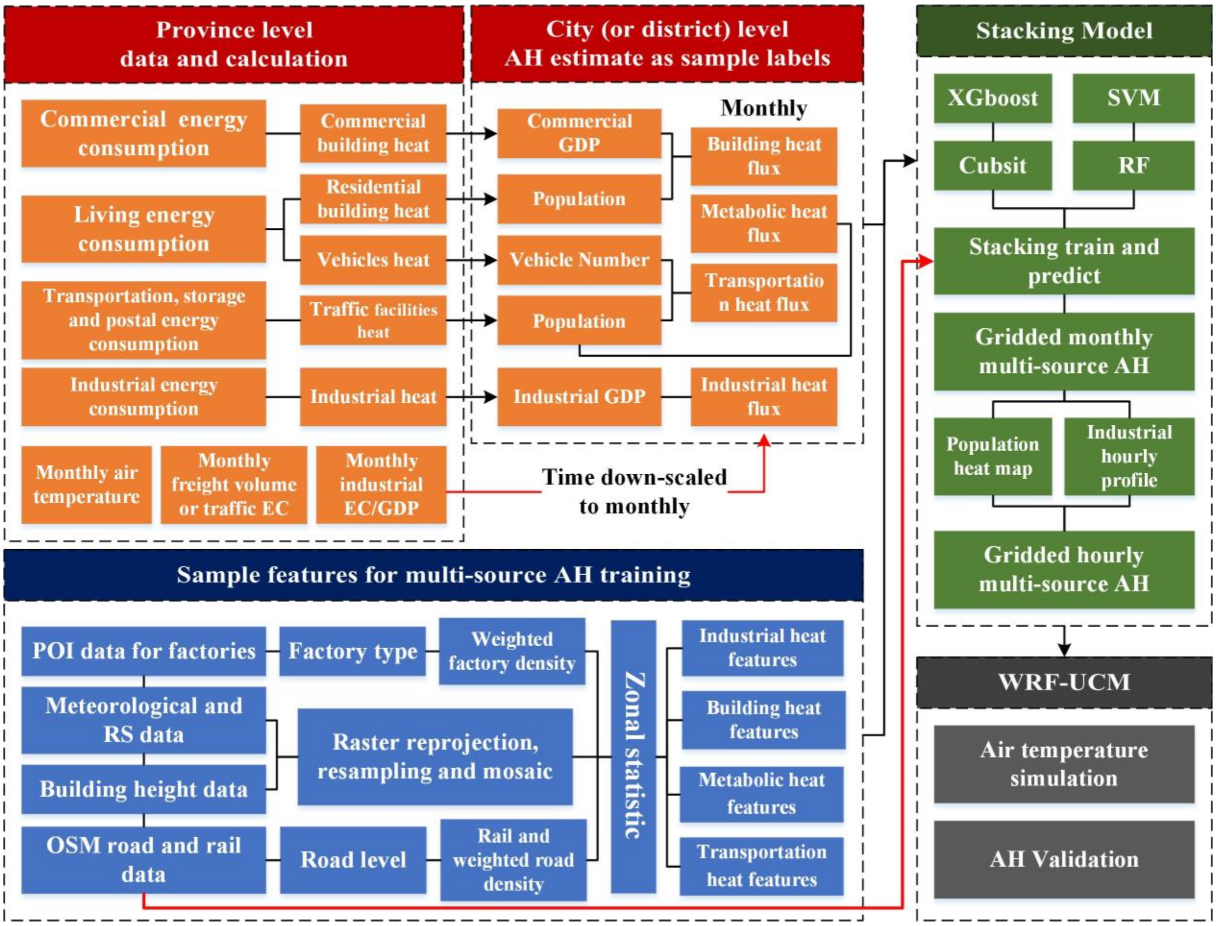

Fig. 2. Technical flow. AH: anthropogenic heat flux; EC: electricity consumption; GDP: gross domestic product; POI: points of interest; OSM: open street map; SVM: support Vector Machine; RF: random forest; XGBoost: extreme Gradient Boosting; WRF-UCM: the Weather Research and Forecasting model coupled with the single-layer urban canopy model. More detailed district-level AH was estimated at the city level in only 12 cities (diagonal grid in **Fig. 1**).

3.1 Corrected AH estimation as sample labels

The top-down energy consumption inventory method is most commonly used for large-scale AH estimation. In this study, the AH was estimated and downscaled based on energy consumption and socioeconomic data to obtain sample labels of AH in administrative areas for model training. Previous studies tended to use living energy consumption from statistical yearbooks to estimate residential building heat emissions, while transportation heat emissions were additionally calculated based on the number of civilian vehicles (Ming et al., 2022; Wang et al., 2019; Wang et al., 2022d). However, such estimates are not reasonable because the energy consumption of civilian vehicles is included in the living energy consumption according to the statistical standards of the National Bureau of Statistics of China (National Bureau of Statistics of China, 2020). In addition, the energy consumption of public transportation facilities should be considered when estimating transportation heat. Therefore, the top-down method used in China must be corrected to obtain more accurate multi-source AH values and compositional ratios. The annual average AH components at the city level including building heat ($\mathrm{Q_B}$), transportation heat ($\mathrm{Q_T}$), industrial heat ($\mathrm{Q_I}$), and metabolic heat ($\mathrm{Q_M}$) with unit $W \cdot \mathrm{m}^{-2}$ were calculated as follows:

$$Q_B = \frac{\varepsilon \times (C_L \times (1-\gamma_v) \times \alpha_p + C_C \times \alpha_c)}{A \times T} \tag{1}$$

$$Q_T = \frac{\varepsilon \times (C_L \times \gamma_v \times \alpha_v + C_T \times \alpha_p)}{A \times T} \tag{2}$$

$$Q_I = \frac{\varepsilon \times C_I \times \alpha_i}{A \times T} \tag{3}$$

$$Q_M = \frac{(H_A \times T_A + H_S \times T_S) \times P}{A \times (T_A + T_S)} \tag{4}$$

where C_L, C_{C}, C_{I}, and C_{T} are provincial energy consumptions (ton of standard coal equivalent, tce) for living, commerce (wholesale, retail, accommodation, and catering), industry, and transportation facilities, respectively; ε is the calorific value of standard coal = 29.3 $\mathrm{MJ} \cdot \mathrm{kg}^{-1}$; γ_v is the proportion (%) of fuel oil consumption to the total living energy consumption of households in four representative regions of China from the statistics of the Chinese General Social Survey 2015; α_p is the proportion of the city's population to the province; α_c is the proportion of the electricity consumption or GDP in the tertiary sector of the city to the province;

α_i is the proportion of the electricity consumption or GDP in the industrial sector; A is the administrative area of the city (m^2); and T is for one year (s). For Q_M, H_A and H_S are the metabolic heat intensities (W) at active and sleepiness times, respectively; T_A and T_S are active and sleep times; P is the total population of the city (Jin et al., 2020).

Owing to the demands of large-scale studies, the calculation of monthly AH weights must be representative while allowing for sufficient data availability. Thus, the monthly AH was calculated using the following equation:

$$Q_{month} = Q_{year} \times \beta_m \tag{5}$$

$$\beta_m = \frac{\delta_m}{(\sum_{m=1}^{12} \delta_m)/12} \tag{6}$$

where Q_{month} is the monthly multi-source AH, Q_{year} is the annual multi-source AH, and β_m is the monthly weight, which was calculated using alternative data δ_m for different heat sources. For Q_B, δ_m can be estimated from the variation pattern of the energy consumption with temperature, as proposed in previous studies (Allen et al., 2011; Liu et al., 2021). For Q_T, δ_m represents the monthly freight volume or transportation electricity consumption and for Q_I, δ_m represents monthly industrial electricity consumption or GDP (Qian et al., 2022). All data and calculations involving monthly weights were conducted on a provincial scale. Owing to the small value of metabolic heat, it was considered to have no monthly variation. The specific data used were determined based on the availability of local statistical data.

In addition, previous large-scale AH samples for China often take the city administrative extent as the unit of calculation (Chen et al., 2020; Wang et al., 2022d); however, due to the large area of the administrative city, the AH label values were low and samples with high label values were absent in the training of the models. In contrast, it is difficult to refine all AH labels to the district level (subordinate to cities) because of data limitations (Qian et al., 2022). Therefore, this study implemented a more efficient scheme by calculating district-level AH sample labels based on a process similar to that described in Eqs. (1)–(6) for China's 12 most developed and representative cities (**Fig. 1**), which, together with the national city level AH, formed 5892 labels, which is a much larger sample size and larger numerical range than in previous studies.

3.2 Improved sample feature processing

It was necessary to select appropriate input variables (sample features) for different AH sources. All features in this study were computed as the average of the city or district administrative boundaries corresponding to the sample labels. Remote sensing data provide large-scale spatiotemporal and attribute information. Common data, such as nighttime lights, daytime and nighttime LST, NDVI, and DEM, were selected based on previous studies (Chen et al., 2020; Qian et al., 2022). Meteorological data, including air temperature, humidity, and wind speed, are important for determining outdoor thermal comfort and the ability of cities to dissipate heat. Therefore, remote sensing and meteorological data were used as common variables for all AH sources. All the gridded data were processed to a resolution of 500 m.

For Q_B modeling, nightlight data can reflect socioeconomic dynamics, population, and energy consumption to some extent (Chen et al., 2015; Varquez et al., 2021). However, the limitations of the remote-sensing observation plane cause bias because height information cannot be reflected. Considering the important association between building height and Q_B

(Liu et al., 2021), we included the 10-meter resolution building height data of China proposed by Wu et al. (2023b). The building raster tiles were resampled to 500 m by grid averaging to match the spatial scale of most of the remote sensing data and were mosaicked over the entire country.

For Q_T, rail and road densities (vector data) can reflect transportation activities; however, the differences between various road levels should be emphasized (Qian et al., 2022). In contrast to separately calculating road densities for different road levels for model training and prediction as done in previous studies (Chen et al., 2020), this study established a weighted road density based on the China Technical Standards of Highway Engineering, which was more convenient and accurate.

For Q_I, it is important to determine the location of factories or industrial zones, which can be located in large-scale studies using POI or night-fire data (Chen et al., 2020; Varquez et al., 2021); however, differences in energy consumption between various factories need to be considered. This study classified all factory POI into light and heavy industries based on the keywords of factory name, and the light industries were further divided into other factories and printing, clothing, and furniture factories, which are more common in city centers. Finally, the weight of each factory type was calculated based on the energy consumption of each industrial sector in China in 2019 and the weighted factory density was calculated. Calculations of the above weights and density raster are provided in the Supplementary Material.

3.3 Model based on Stacking framework

After preparing the samples, a machine-learning model was built to represent the relationship between the features and the AH. Previous studies have revealed differences in the performances of various algorithms for estimating different AH sources (Qian et al., 2022). Therefore, integrating multiple algorithms might improve the estimation of multi-source AH by reducing errors owing to algorithm applicability. The stacking used in this study is a hierarchical ensemble framework (Wolpert, 1992) that effectively improves the accuracy of the machine learning models. Specifically, the commonly used extreme gradient boosting (XGBoost), random forest (RF), support vector machine (SVM), and cubist models in the field of urban thermal environments were selected to form the base model for the stacking framework (Chen et al., 2020; Chen et al., 2022a; Gao et al., 2022; Mathew et al., 2019). New training features were constructed based on a five-fold cross-validation. Multivariable linear regression, a simple algorithm, was used to train the second-layer model to integrate the results of the base models (Qian et al., 2023).

The monthly gridded AH can be obtained from the stacking model using raw data input and further downscaled in time to the hourly AH:

$$AH^h = f_P^h \cdot Q_B^m + f_P^h \cdot Q_T^m + f_I^h \cdot Q_I^m + Q_M^h \quad (7)$$

$$f_P^h(City) = \frac{Ph_h}{\sum_{h=0}^{23} Ph_h / 24} \quad (8)$$

$$f_P^h(Region) = mean\big(f_P^h(City) \neq 1\big) \quad (9)$$

Where Q_B^m, Q_T^m, and Q_I^m are the monthly building, transportation, and industrial heat flux outputs from the stacking model, respectively; and f_P^h is the hourly weight calculated based on the population heat value Ph_h, with h representing a specific hour. Population heat data are based on the geographical location data of mobile phone users and can characterize the distribution of people across a city in real time. Therefore, population heat data were used to represent the diurnal variation in building and transportation heat. For the seven representative cities for which population heat data were available (Qian et al., 2023), $f_P^h(City)$ represents gridded data with spatial heterogeneity. For regions where population heat data were unavailable across the country, $f_P^h(Region)$ was a single value of the specific region shown in different colors (**Fig. 1**), indicating that the mean of the pixels with the $f_P^h(City)$ was not equal to 1 within the representative city corresponding to the region and was only applied to image pixels with annual AH greater than 1. f_I^h is the hourly weight of industrial heat proposed in previous studies (Liu et al., 2021; Zheng and Weng, 2018).

3.4 Validation based on regional climate simulations

By considering the important influence of AH on the regional climate, simulations of meteorological factors can be used to assess the accuracy of AH inputs. The Weather Research and Forecasting (WRF) model is a state-of-the-art mesoscale numerical weather prediction system designed for both atmospheric research and operational forecasting applications. WRF version 4.4 was used in this study. The exchange of energy and momentum between the urban surface and atmosphere was implemented in the WRF model coupled with the single-layer urban canopy model (Kusaka and Kimura, 2004), which considers AH released in the form of sensible heat. In addition to the results of this study, the default AH values of the WRF and AH datasets from previous studies (Chen et al., 2020; Varquez et al., 2021; Wang et al., 2022c) were used for sensitivity analysis. In addition, the Noah land surface model (Tewari et al., 2004), WRF Single-Moment six-class microphysics scheme (Hong and Lim, 2006), Rapid Radiative Transfer Model for General Circulation Models longwave and shortwave radiation scheme (Iacono et al., 2008), Revised MM5 Monin–Obukhov surface layer scheme (Jiménez et al., 2012), and Yonsei University planetary boundary layer scheme (Tewari et al., 2004) composed the model physics. We set up three two-way nested domains with grid spacings of 25, 5, and 1 km, with the innermost domain covering the main urban area of Beijing. The simulation periods were 00:00 UTC January 18, 2019, to 00:00 UTC January 25, 2019, with the first 6 h of simulations considered as model spin-up. The 3-hourly $0.25° \times 0.25°$ ERA5 surface and pressure layer reanalysis provided the WRF initial and boundary conditions. The root mean square error (RMSE) was used as an assessment metric.

4. Results

4.1 AH composition and model assessment

AH emissions varied considerably between provinces (**Fig. 3**) and provinces with larger economies generally had larger heat emissions; however, this relationship was not uniform. Among the selected provinces, Shandong had the highest total heat emissions, whereas Beijing had the lowest. In particular, Hebei and Liaoning had lower economic volume but their energy consumption and heat emissions were very high owing to the large proportion of heavy industry. Considerable differences were observed in AH composition between the provinces. In general, industrial heat accounted for the largest proportion (> 50 %) of AH in most provinces, followed by building and transportation heat, whereas metabolic heat accounted for a very small proportion. However, in Beijing and Shanghai, the proportion of industrial heat was relatively low, particularly in Beijing, where both building and transportation heat accounted for more than 30%.

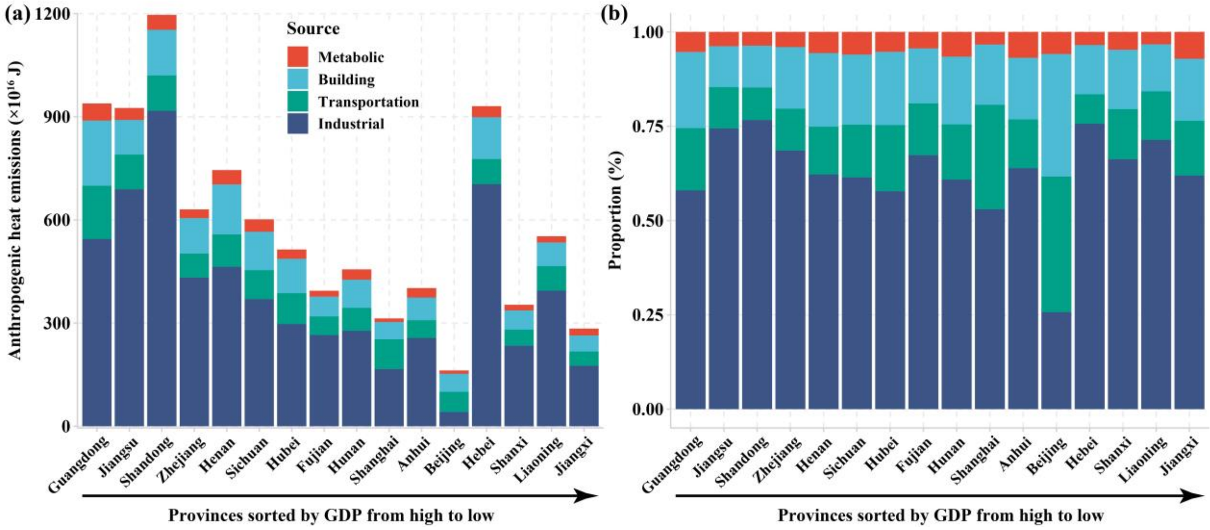

Fig. 3. Total annual multi-source AH emission (a) amount (J) and (b) proportion (%).

All models except for SVM had low errors and the performance of the models varied for different AH sources and error criteria (**Table 1**). Although the SVM model had a large estimation error owing to its relatively simple algorithmic structure, its low correlation with other algorithms increased stacking effectiveness which requires heterogeneity between algorithms. XGboost had a smaller RMSE but larger mean absolute error (MAE) in the building and industrial heat estimates compared to other algorithms, Cubist had a smaller RMSE and MAE in the transportation estimate, and RF performed better in MAE. In contrast to the single models, for which it was difficult to judge the performance simply, the stacking model performed better in general, with the RMSE and MAE being better than or close to the best single model in each AH source estimation.

Table 1. Root mean squared errors (RMSE) and mean absolute errors (MAE) for different model training

	RMSE/MAE		
Model	Building heat	Industrial heat	Transportation heat
XGboost	0.48/0.19	1.68/0.72	0.83/0.27
RF	0.52/0.16	1.76/0.58	0.90/0.23
Cubist	0.53/0.18	1.82/0.61	0.75/0.21
SVM	1.41/0.60	6.26/2.12	3.04/1.00
Stacking	0.40/0.15	1.48/0.56	0.70/0.21

Different features played different roles in the estimation (**Fig. 4**). Specifically, the building height, improved weighted factory density, and weighted road network density considered in this study played the largest roles in the estimation of building heat, industrial heat, and transportation heat, respectively, whereas nighttime lights were the second most important feature for all AH sources. Furthermore, temperature, humidity, and wind speed, which are variables that express meteorological conditions, play more significant roles in building heat estimation. Although the factor features used to distinguish between different months were of little help in the estimation, the role of regional factor features cannot be overlooked.

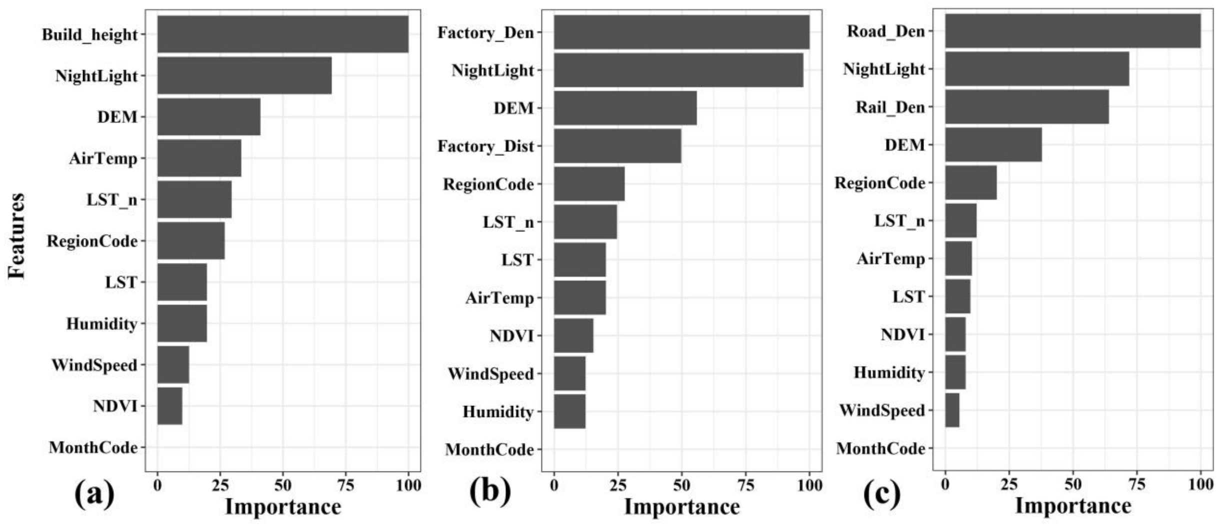

Fig. 4. Importance of the features for (a) building heat, (b) industrial heat, and (c) transportation heat. Factory_Den: weighted factory density; Factory_Dist: distance from the factories; Road_Den: weighted

road density; LST_n: nighttime LST; RegionCode: factor features to represent different regions of **Fig. 1** in color; MonthCode: factor features to represent 12 months.

4.2 Spatial characteristics of AH

AH in China was most strongly concentrated in the Yangtze River Delta, Pearl River Delta, and Beijing-Tianjin-Hebei regions, followed by the surrounding areas of megacities such as Chengdu, Chongqing, and Wuhan. Eastern China had a remarkable dominance of AH, whereas AH was very weak in large areas of Western China and different AH sources showed notably diverse spatial distribution characteristics (**Fig. 5** and **Fig. 6**). The value of building heat was small, although widely distributed; the high values were concentrated in the built-up area of the urban centers and gradually diminished outward. Its spatial distribution characteristics were similar to those of metabolic heat but the value of metabolic heat was much smaller. Transportation heat was distributed linearly along roads and rails, with high intensity near major routes in urban centers. However, its spatial distribution was less extensive and almost absent in areas away from major transportation routes. Industrial heat had the highest intensity overall, with irregular distribution in the form of scattered dots, which largely depended on the location of factories or industrial zones. In contrast to the strong concentrations of building and transportation heat in city centers, industrial heat was widely distributed in the suburbs and rural areas with high intensity.

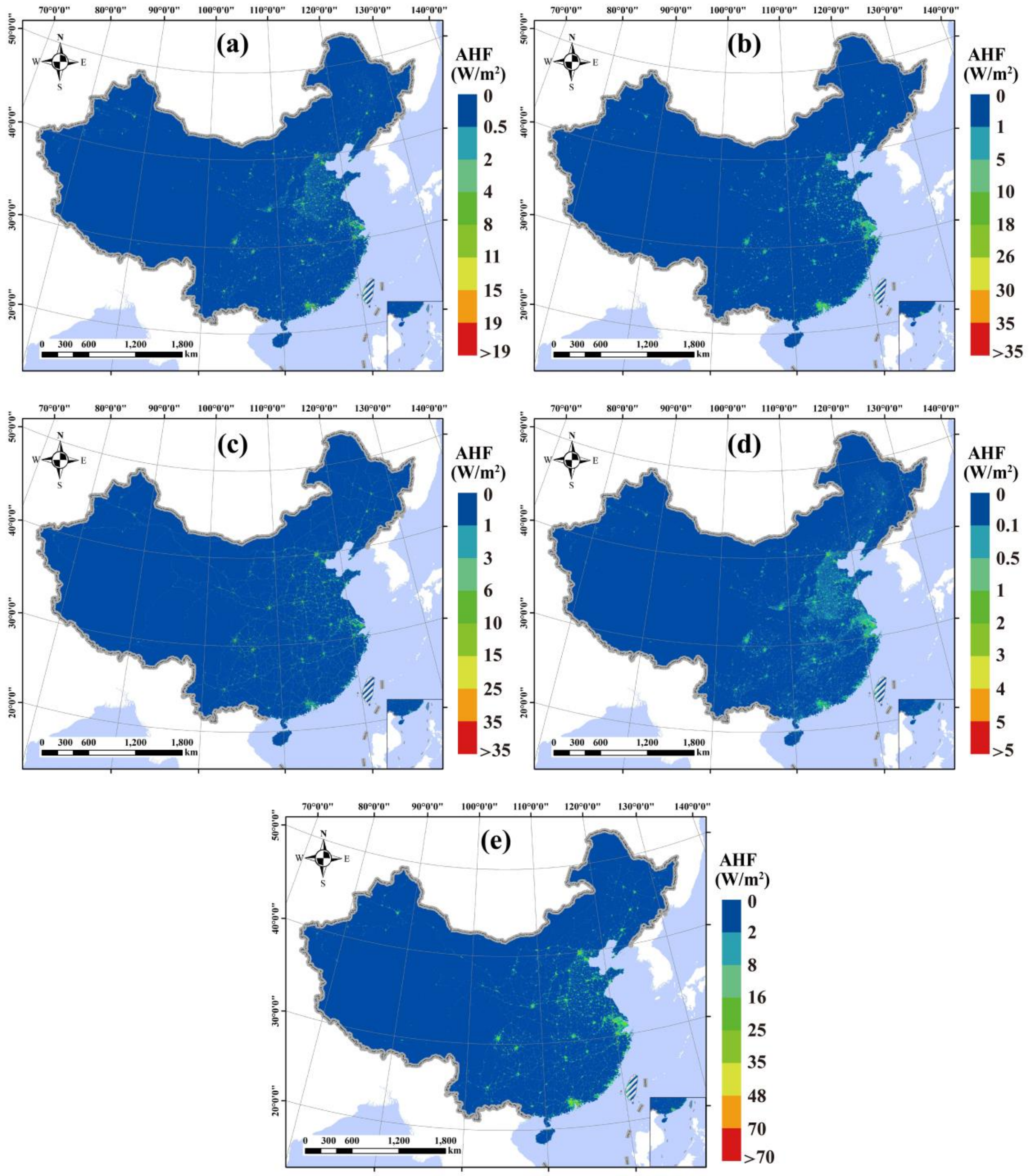

Fig. 5. (a) Building heat flux, (b) industrial heat flux, (c) transportation heat flux, (d) metabolic heat, and (d) total heat flux in China. The slash lines indicate partial missing data for Taiwan.

4.3 Temporal variations of AH

This study achieved detailed temporal characteristics of AH at a large spatial scale. Building heat varied notably across months and latitudinal regions (**Fig. 6**). The intensity of building heat was the highest during the cold winter (January) due to the centralized heating requirements of Beijing, followed by the summer (July), and was weak during the spring and autumn months when temperatures were relatively comfortable. In the hot summer months, building heat peaked in Shanghai and Guangzhou. In contrast, during winter, building heat was high in Shanghai but was at the lowest level of the year in Guangzhou, which has a mild winter climate. In contrast to building heat, monthly variations in transportation and industrial heat were not evident and the characteristics of the variations did not differ significantly among cities. The hourly variation patterns of AH in Shanghai and Beijing were similar (**Fig. 7**), with the lowest values from 3:00 to 4:00 midnight, followed by a gradual recovery and peak at approximately 9:00 a.m. High AH values remained until 9:00, when a notable decreasing trend began.

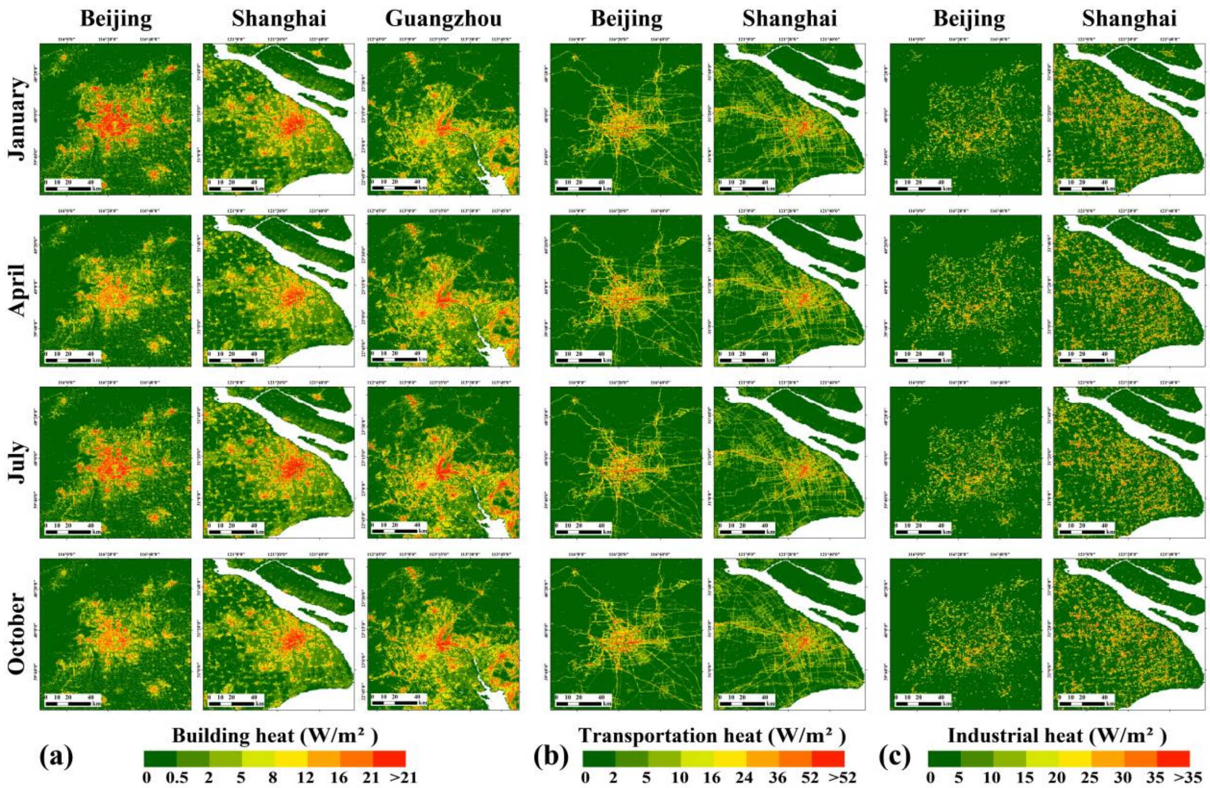

Fig. 6. Monthly (a) building heat, (b) transportation heat, and (c) industrial heat in case cities.

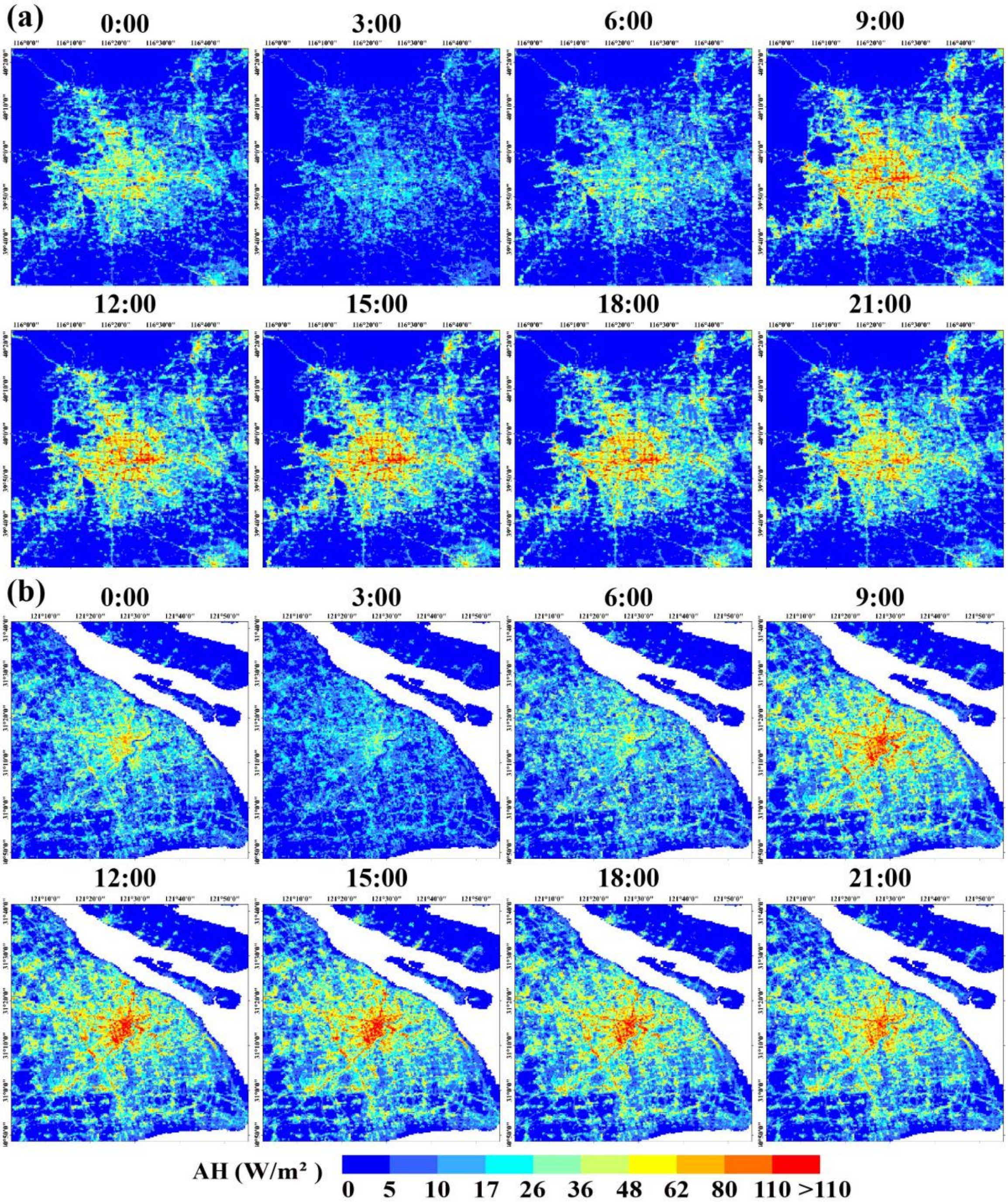

Fig. 7. Local time hourly AH in (a) Beijing and (b) Shanghai in April.

4.4 Comparison and validation

Comparing with previous results remains the most important validation approach for current AH studies. Large-scale studies lacking fine temporal characteristics or representing study periods from many years ago were excluded from the comparison. Thus, only a few recent studies on annual AH were compared (**Fig. 8**). The spatial characteristics of building heat, transportation heat, and industrial heat estimated by Chen et al. (2020) were similar to those determined in this study in that they gradually diminished from the city center outward. However, the results of the present study have finer spatial details and contrasting characteristics for different AH sources. Our determined characteristics of building heat were similar to those of previous studies but the linear distribution of transportation heat was more obvious. In particular, the industrial heat in this study was not characterized by a distribution clustered in the urban center, as in previous studies, but was irregularly and widely distributed within the city administrative areas and even weakly distributed in the urban center. The total AH in this study was similar to the results of Wang et al. (2022c) which were based on a linear relationship with nighttime lighting. However, in airports (e.g., the northeast corner of Beijing and the easternmost part of Shanghai), the results of Wang et al. (2022c) had anomalously high values, which were absent in this study.

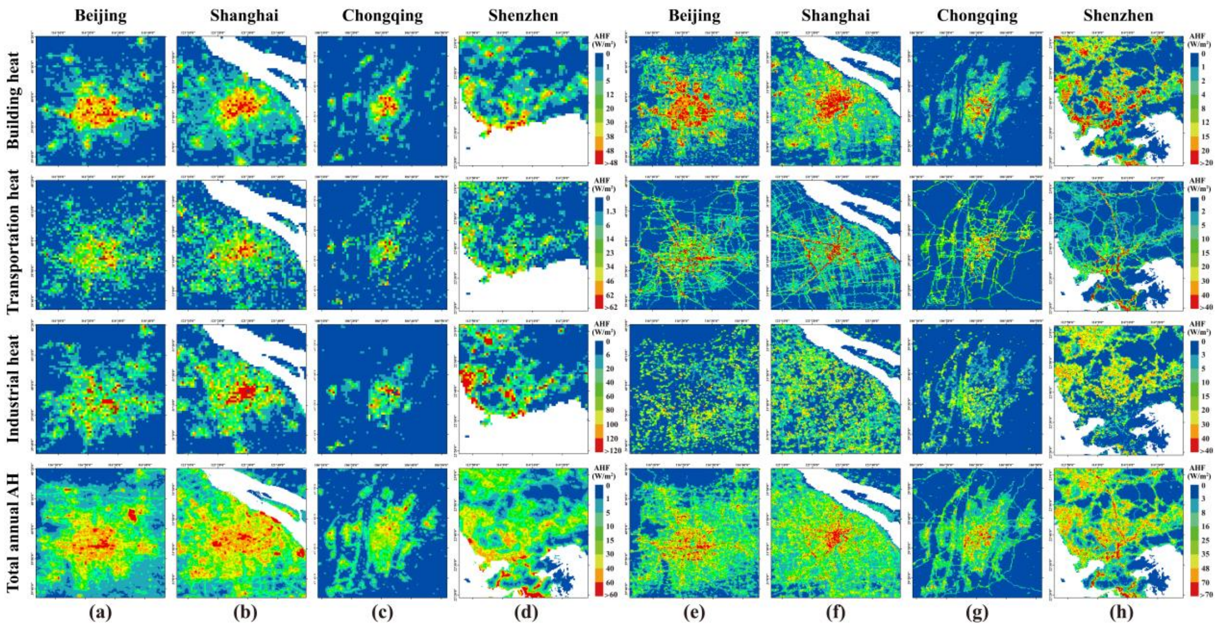

Fig. 8. Comparison with the results of previous studies: (a)-(d) are previous estimates of building heat, transportation heat, industrial heat (Chen et al., 2020) and the total annual average AH (Wang et al., 2022c); (e)-(f) are the results of this study.

The accuracy of the AH spatial and temporal characteristics was further determined through climate simulations of the WRF and comparison with station observations (**Fig. 9**). Air temperature simulations in Beijing during winter showed the optimization effect of AH inputs on the numerical climate model. Compared with the default AH parameters of the WRF and the results of previous studies, the spatiotemporal heterogeneous AH inputs from this study improved the simulation accuracy the most, followed by the results of Chen et al. (2020), who obtained a similar simulation accuracy. In contrast, the results of Wang et al. (2022b) were close to the default AH of the WRF. Although the simulation accuracy of Varquez et al. (2021) was lower than that of the default AH input, it was still better than that of the scenario without AH.

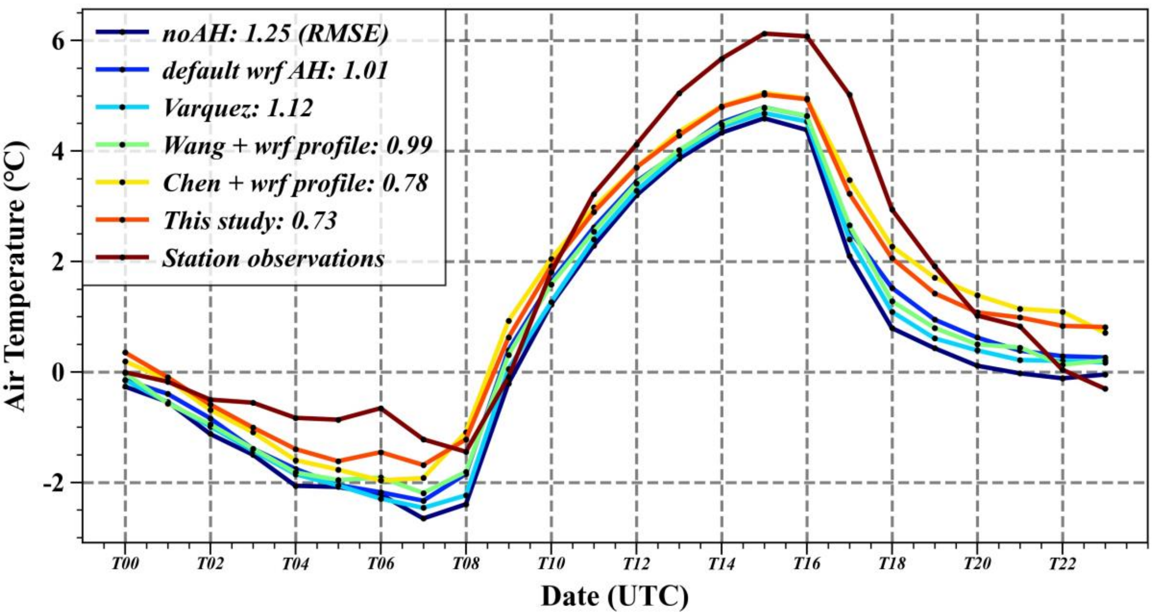

Fig. 9. AH sensitivity analysis based on the average diurnal temperature in Beijing winter. The RMSE represents the mean error between observed and simulated temperatures at the station locations..

5. Discussion

5.1 Implications for improvements

5.1.1 More accurate and detailed characteristics

This study made improvements to the energy consumption inventory method, machine-learning sample features, and model training. Unlike previous top-down approaches conducted in China (Ming et al., 2022; Wang et al., 2019; Yu et al., 2021a), this study distinguished residential building and civilian vehicle energy consumption in the living energy consumption based on the statistical standards of the National Bureau of Statistics of China and considered the energy consumption of public transportation facilities so that transportation heat was not additionally calculated based on the number of vehicles. This improvement is theoretically valid because of the more critical and adequate understanding of energy consumption data based on the information we got from the Bureau of Statistics. Unlike Wang et al. (2019), this study adjusted the proportion of transportation heat in the total AH, which made the proportion of multi-source AH more reasonable and corrected the overestimation of total AH (**Fig. 3**). This is an update of the basic AH estimation method from a deep dive into the official energy consumption data of China, which establishes a more convenient and exact standardized process of energy consumption inventory method estimation to adapt to the increasing complexity of the AH quantification requirements (Meng et al., 2023).

This study improved the sample feature selection and processing for the spatial characteristics of different AH sources. For building heat estimation, nighttime lighting is the most commonly used spatial proxy (Dong et al., 2017; He et al., 2020; Wang et al., 2022c). Although nighttime lighting is still very important in the modeling process, its inability to express the information of building heights and densities is a limitation. Our results demonstrated the importance of building height data (**Fig. 4**). The spatial and attribute information contained in building height data also made the gridded building heat in this study more refined than that of Chen et al. (2020). In addition, the involvement of building information overcomes the abnormally high AH in areas such as airports and harbors owing to high lighting at night (Wang et al., 2019; Wang et al., 2022c), making the estimations in these areas agree more closely with the AH should be expected from their building heights and densities (**Fig. 8**). Measuring the actual traffic volumes on different roads is extremely difficult, especially in large-scale studies (Qian et al., 2023). However, this study utilized road design criteria to assign weights for different levels of roads so that the weighted road densities could be used to reflect the general transportation activity intensity on different roads, which greatly simplified data processing and model complexity and obtained satisfactory results. The results finely characterized the transportation heat distribution within the city, with high consistency with relevant small-scale studies (Ming et al., 2022; Sun et al., 2018). The importance of weighted road density also confirmed its usefulness. In our analysis, industrial heat was the most different component compared to previous studies (**Fig. 8**). And the improvement in the accuracy of POI data from Amap for the spatial characteristics of industrial heat has been illustrated in previous studies (Qian et al., 2022). The weighted factory density had the greatest importance in industrial heat estimation and was calculated based on the energy consumption of different types of factories. The special locational requirements of factories and industrial zones implied that the spatial distribution characteristics of industrial heat were distinctly different from those of building and transportation heat. The industrial heat should be low in urban centers where population and commercial activities are concentrated, which was clearly expressed by the present results (**Fig. 8**). But previous studies (Chen et al., 2020; Varquez et al., 2021) did not avoid the overestimation of industrial heat in urban centers.

Another novelty of the present investigation is the detailed temporal characterization obtained simultaneously with a large spatial extent study (**Fig. 6** and **Fig. 7**). Compared to the results of Varquez et al. (2021), who also obtained hourly AH, the present study achieved a higher spatial resolution and more accurate spatial characteristics, used more recent data, and performed better in climate simulations (**Fig. 9**). The AH spatiotemporal variability characterized in this study achieved a similar degree of detail to refined studies at small spatial scales (Liu et al., 2021; Sun et al., 2018; Xu et al., 2021), which is rare in other current large-scale AH datasets. In summary, the improvements in this study were effective and realized an accurate multi-source AH estimation that considered both large extent and fine spatiotemporal characteristics. The resulting dataset is one of the latest and most accurate AH datasets available for China.

5.1.2 Implications for climate simulations

The remarkable effects of AH on climate and air quality in urban areas have been widely demonstrated (Yang et al., 2019; Zhan and Xie, 2022) and more accurate spatially heterogeneous AH data can optimize the precision of simulations of meteorological elements and pollutants (Molnar et al., 2020; Wang et al., 2023; Xie et al., 2016). Therefore, the quantitative validation of AH models based on climate simulations is theoretically justified and the results of this study show that the input of sophisticated spatiotemporal AH is beneficial (**Fig. 9**). Although the AH4GUC dataset of Varquez et al. (2021) possesses sufficient spatiotemporal resolution, their data for 2010 are out-of-date, resulting in a simulation performance lower than that of the default fixed AH in WRF. The AH data for 2016 from Wang et al. (2022b) have a 500 m resolution, which is consistent with the data in the present study; however, its simulation precision is only moderate because of the lack of time features and multi-source AH differences. The multi-source AH dataset of Chen et al. (2020), also built based on machine learning, had the second lowest simulation error when coupled with the WRF default hourly AH profile (**Fig. 9**); however, its original dataset lacks temporal variability and thus requires a combination of external information for practical applications. In contrast to the above datasets, the AH results in the present study achieved a temporal resolution as fine as hours on the grids, with unique characteristics of temporal variations in each grid, and more detailed and accurate spatial characteristics for the different AH sources. This resulted in temperature simulations with the highest accuracy. Overall, improved AH inputs are important for optimizing the accuracy of climate simulations. In addition to more accurate spatial and temporal characteristics, attention should be paid to the timely use of AH data, especially in regions with fast economic development. Based on more accurate AH datasets and meteorological numerical models, the impact of human activities can be further clarified to optimize urban planning and settlement environments. However, the requirements of high computing power and long runtime for numerical simulations are key issues that must be considered.

5.2 Limitations and prospects

This study provides effective improvements in many aspects of AH modeling; however, many problems remain to be overcome by subsequent research. Although the hourly AH was estimated, further consideration of the intraday variation differences between weekdays and weekends should be given. If supported by sufficient data, quantification of AH for multiple scenarios can be achieved with different change characteristics for weekdays, holidays, and weekends. Another important issue is that changes in AH from centralized heating in winter in northern areas are difficult to reflect using indicators of population activity intensity, which is a problem that the current field has not overcome, especially in large-scale studies. In the future, if detailed heating energy consumption data can be obtained to establish the corresponding typical building heat emission change criteria, these can be applied to large-scale studies. Finally, there is room for improvement in the ability of machine learning models for AH to recognize features in particular regions. For example, the large heavy industrial energy consumption in Shandong was not well reflected in this study and required more accurate geographic information data of factories. In addition, how to apply these fine data in large spatial scale studies is also a key consideration for future studies.

6. Conclusion

This study estimated annual, monthly, and hourly AH of multiple heat sources with fine spatial and temporal characteristics in China for 2019. Specifically, this study corrected the irrational application of the top-down energy consumption inventory method for China, optimized the AH modeling process of machine learning, improved the selection and processing of sample features for different AH sources, and refined the results of large-scale AH estimation to finer time scales. The results showed that industrial heat accounted for the highest proportion of AH but the composition of AH in different regions varied notably. The sample features added or improved in this study, including building height, weighted road network density, and weighted factory density, all played the strongest roles in the modeling of the different AH sources. The stacking model effectively solved the optimal algorithm selection problem and improved the modeling accuracy. High values of AH in China were concentrated in the Yangtze River Delta, Pearl River Delta, and Beijing-Tianjin-Hebei regions but the spatial characteristics of the different AH sources were markedly distinct. Building heat showed a distinct monthly variation and was related to climate and latitude, whereas industrial heat and transportation heat showed almost no variation throughout the year. The hourly changes in AH were consistent with the general patterns of human work and rest. The spatial and temporal characteristics of the multi-source AH obtained in this study were more accurate and finer than those in previous studies and better accuracy was achieved in regional climate simulations, which is rare for large-scale multi-temporal multi-source AH datasets.

This study established a complete and standardized framework from basic AH estimation methods to related model training, which can effectively integrate the currently abundant data for application in large-scale AH studies. This study provided a reliable foundation for further refinement of the AH dataset and more accurate data inputs for regional climate simulations, thus promoting a deeper understanding of the urban thermal environment and supporting sustainable urban development and rational utilization of energy consumption.

Acknowledgement

This work was funded by the National Natural Science Foundation of China Major Program [grant numbers 42192580, 42192584]; the National Natural Science Foundation of China [grant numbers 42201384]; the FY-3 Lot 03 Meteorological Satellite Engineering Ground Application System Ecological Monitoring and Assessment Application Project (Phase I) (grant numbers ZQC-R22227); the Youth Innovation Promotion Association CAS (grant numbers 2023139).

Reference

Alhazmi, M., Sailor, D.J., Anand, J., 2022. A new perspective for understanding actual anthropogenic heat emissions from buildings. Energy Build. 258, 111860. https://doi.org/10.1016/j.enbuild.2022.111860

Allen, L., Lindberg, F., Grimmond, C.S.B., 2011. Global to city scale urban anthropogenic heat flux: model and variability. Int. J. Climatol. 31, 1990-2005. https://doi.org/10.1002/joc.2210

[dataset] Amy, McNally, NASA/GSFC/HSL, 2018. FLDAS Noah Land Surface Model L4 Global Monthly 0.1 x 0.1 degree (MERRA-2 and CHIRPS). Greenbelt, MD, USA, Goddard Earth Sciences Data and Information Services Center (GES DISC). 10.5067/5NHC22T9375G

Chen, B., Zhao, J.Q., Chen, L.F., Shi, G.Y., 2015. Anthropogenic heat release: Estimation of global distribution and possible climate effect. J. Meteorol. Soc. Jpn. 93, 645-645. https://doi.org/10.2151/jmsj.2015-060

Chen, Q., Yang, X., Ouyang, Z., Zhao, N., Jiang, Q., Ye, T., Qi, J., Yue, W., 2020. Estimation of anthropogenic heat emissions in China using Cubist with points-of-interest and multisource remote sensing data. Environ. Pollut. 266, 115183. https://doi.org/10.1016/j.envpol.2020.115183

Chen, S., Yang, Y., Deng, F., Zhang, Y., Liu, D., Liu, C., Gao, Z., 2022a. A high-resolution monitoring approach of canopy urban heat island using a random forest model and multi-platform observations. Atmospheric Measurement Techniques 15, 735-756. https://doi.org/10.5194/amt-15-735-2022

Chen, W., Zhou, Y.Y., Xie, Y.H., Chen, G., Ding, K.J., Li, D., 2022b. Estimating spatial and temporal patterns of urban building anthropogenic heat using a bottom-up city building heat emission model. Resour. Conserv. Recycl. 177, 105996. https://doi.org/10.1016/j.resconrec.2021.105996

Chow, W.T.L., Salamanca, F., Georgescu, M., Mahalov, A., Milne, J.M., Ruddell, B.L., 2014. A multi-method and multi-scale approach for estimating city-wide anthropogenic heat fluxes. Atmos. Environ. 99, 64-76. https://doi.org/10.1016/j.atmosenv.2014.09.053

Cong, J.P., Wang, L.B., Liu, F.J., Qian, Z.M., McMillin, S.E., Vaughn, M.G., Song, Y.M., Wang, S.S., Chen, S.S., Xiong, S.M., Shen, X.B., Sun, X., Zhou, Y.Z., Ho, H.C., Dong, G.H., 2022. Associations between metabolic syndrome and anthropogenic heat emissions in northeastern China. Environ. Res. 204, 111974. https://doi.org/10.1016/j.envres.2021.111974

Dong, Y., Varquez, A.C.G., Kanda, M., 2017. Global anthropogenic heat flux database with high spatial resolution. Atmos. Environ. 150, 276-294. https://doi.org/10.1016/j.atmosenv.2016.11.040

Ferreira, M.J., de Oliveira, A.P., Soares, J., 2011. Anthropogenic heat in the city of So Paulo, Brazil. Theor. Appl. Climatol. 104, 43-56. https://doi.org/10.1007/s00704-010-0322-7

Firozjaei, M.K., Weng, Q.H., Zhao, C.H., Kiavarz, M., Lu, L.L., Alavipanah, S.K., 2020. Surface anthropogenic heat islands in six megacities: An assessment based on a triple-source surface energy balance model. Remote Sens. Environ. 242, 111751.

https://doi.org/10.1016/j.rse.2020.111751
Flanner, M.G., 2009. Integrating anthropogenic heat flux with global climate models. Geophysical Research Letters 36, 4.
Gao, J.F., Meng, Q.Y., Zhang, L.L., Hu, D., 2022. How does the ambient environment respond to the industrial heat island effects? An innovative and comprehensive methodological paradigm for quantifying the varied cooling effects of different landscapes. Giscience & Remote Sensing 59, 1643-1659. https://doi.org/10.1080/15481603.2022.2127463
Grimmond, C.S.B., 1992. THE SUBURBAN ENERGY-BALANCE - METHODOLOGICAL CONSIDERATIONS AND RESULTS FOR A MIDLATITUDE WEST-COAST CITY UNDER WINTER AND SPRING CONDITIONS. Int. J. Climatol. 12, 481-497. https://doi.org/10.1002/joc.3370120506
Hamilton, I.G., Davies, M., Steadman, P., Stone, A., Ridley, I., Evans, S., 2009. The significance of the anthropogenic heat emissions of London's buildings: A comparison against captured shortwave solar radiation. Build. Environ. 44, 807-817. https://doi.org/10.1016/j.buildenv.2008.05.024
Han, B., Luo, Z., Liu, Y., Zhang, T., Yang, L., 2022. Using Local Climate Zones to investigate Spatio-temporal evolution of thermal environment at the urban regional level: A case study in Xi'an, China. Sust. Cities Soc. 76, 103495. https://doi.org/10.1016/j.scs.2021.103495
He, C., Zhou, L., Yao, Y., Ma, W., Kinney, P.L., 2020. Estimating spatial effects of anthropogenic heat emissions upon the urban thermal environment in an urban agglomeration area in East China. Sust. Cities Soc. 57, 102046. https://doi.org/10.1016/j.scs.2020.102046
Hertel, D., Schlink, U., 2022. Entropy frameworks for urban heat storage can support targeted adaptation strategies. Urban CLim. 42, 101129. https://doi.org/10.1016/j.uclim.2022.101129
Hong, S.-Y., Lim, J.-O.J., 2006. The WRF single-moment 6-class microphysics scheme (WSM6). Asia-Pac. J. Atmos. Sci. 42, 129-151.
Iacono, M.J., Delamere, J.S., Mlawer, E.J., Shephard, M.W., Clough, S.A., Collins, W.D., 2008. Radiative forcing by long-lived greenhouse gases: Calculations with the AER radiative transfer models. J. Geophys. Res.-Atmos. 113, D13103. https://doi.org/10.1029/2008jd009944
Iamarino, M., Sean, B., Grimmond, C.S.B., 2012. High-resolution (space, time) anthropogenic heat emissions: London 1970–2025. Int. J. Climatol. 32, 1754-1767.
Jiménez, P.A., Dudhia, J., González-Rouco, J.F., Navarro, J., Montávez, J.P., García-Bustamante, E., 2012. A revised scheme for the WRF surface layer formulation. Monthly weather review 140, 898-918.
Jin, K., Wang, F., Chen, D., Liu, H., Ding, W., Shi, S., 2019. A new global gridded anthropogenic heat flux dataset with high spatial resolution and long-term time series. Sci. Data 6, 139. https://doi.org/10.1038/s41597-019-0143-1
Jin, K., Wang, F., Wang, S., 2020. Assessing the spatiotemporal variation in anthropogenic heat and its impact on the surface thermal environment over global land areas. Sust. Cities Soc. 63, 102488. https://doi.org/10.1016/j.scs.2020.102488

Kato, S., Yamaguchi, Y., 2005. Analysis of urban heat-island effect using ASTER and ETM+ Data: Separation of anthropogenic heat discharge and natural heat radiation from sensible heat flux. Remote Sens. Environ. 99, 44-54. https://doi.org/10.1016/j.rse.2005.04.026
Kim, Y., Yeo, H., Kim, Y., 2022. Estimating urban spatial temperatures considering anthropogenic heat release factors focusing on the mobility characteristics. Sust. Cities Soc. 85, 104073. https://doi.org/10.1016/j.scs.2022.104073
Kotthaus, S., Grimmond, C.S.B., 2012. Identification of Micro-scale Anthropogenic CO2, heat and moisture sources - Processing eddy covariance fluxes for a dense urban environment. Atmos. Environ. 57, 301-316. https://doi.org/10.1016/j.atmosenv.2012.04.024
Kusaka, H., Kimura, F., 2004. Coupling a single-layer urban canopy model with a simple atmospheric model: Impact on urban heat island simulation for an idealized case. J. Meteorol. Soc. Jpn. 82, 67-80. https://doi.org/10.2151/jmsj.82.67
Liu, X., Yue, W.Z., Zhou, Y.Y., Liu, Y., Xiong, C.S., Li, Q., 2021. Estimating multi-temporal anthropogenic heat flux based on the top-down method and temporal downscaling methods in Beijing, China. Resour. Conserv. Recycl. 172, 105682. https://doi.org/10.1016/j.resconrec.2021.105682
Mathew, A., Sreekumar, S., Khandelwal, S., Kumar, R., 2019. Prediction of land surface temperatures for surface urban heat island assessment over Chandigarh city using support vector regression model. Solar Energy 186, 404-415. https://doi.org/10.1016/j.solener.2019.04.001
Meng, Q., Qian, J., Schlink, U., Zhang, L., Hu, X., Gao, J., Wang, Q., 2023. Anthropogenic heat variation during the COVID-19 pandemic control measures in four Chinese megacities. Remote Sens. Environ. 293, 113602. https://doi.org/10.1016/j.rse.2023.113602
Ming, Y.J., Liu, Y., Liu, X., 2022. Spatial pattern of anthropogenic heat flux in monocentric and polycentric cities: The case of Chengdu and Chongqing. Sust. Cities Soc. 78, 103628. https://doi.org/10.1016/j.scs.2021.103628
Molnar, G., Kovacs, A., Gal, T., 2020. How does anthropogenic heating affect the thermal environment in a medium-sized Central European city? A case study in Szeged, Hungary. Urban CLim. 34, 100673. https://doi.org/10.1016/j.uclim.2020.100673
[dataset] NASA JPL, 2020. NASADEM Merged DEM Global 1 arc second. NASA EOSDIS Land Processes DAAC, V001. https://doi.org/10.5067/MEaSUREs/NASADEM/NASADEM_HGT.001
[dataset] National Bureau of Statistics of China, 2020. Chinese Statistical Yearbook 2020. China, National Bureau of Statistics of China. http://www.stats.gov.cn/tjsj/ndsj/
Offerle, B., Grimmond, C.S.B., Fortuniak, K., 2005. Heat storage and anthropogenic heat flux in relation to the energy balance of a central European city centre. Int. J. Climatol. 25, 1405-1419. https://doi.org/10.1002/joc.1198
Peng, T., Sun, C., Feng, S., Zhang, Y., Fan, F., 2021. Temporal and Spatial Variation of Anthropogenic Heat in the Central Urban Area: A Case Study of Guangzhou, China. ISPRS Int. Geo-Inf. 10, 160. https://doi.org/10.3390/ijgi10030160

Pigeon, G., Legain, D., Durand, P., Masson, V., 2007. Anthropogenic heat release in an old European agglomeration (Toulouse, France). Int. J. Climatol. 27, 1969-1981. https://doi.org/10.1002/joc.1530

Qian, J., Meng, Q., Zhang, L., Hu, D., Hu, X., Liu, W., 2022. Improved anthropogenic heat flux model for fine spatiotemporal information in Southeast China. Environ. Pollut. 299, 118917. https://doi.org/10.1016/j.envpol.2022.118917

Qian, J.K., Meng, Q.Y., Zhang, L.L., Schlink, U., Hu, X.L., Gao, J.F., 2023. Characteristics of anthropogenic heat with different modeling ideas and its driving effect on urban heat islands in seven typical Chinese cities. Sci. Total Environ. 886, 163989. https://doi.org/10.1016/j.scitotenv.2023.163989

Quah, A.K.L., Roth, M., 2012. Diurnal and weekly variation of anthropogenic heat emissions in a tropical city, Singapore. Atmos. Environ. 46, 92-103. https://doi.org/10.1016/j.atmosenv.2011.10.015

Sailor, D.J., 2011. A review of methods for estimating anthropogenic heat and moisture emissions in the urban environment. Int. J. Climatol. 31, 189-199. https://doi.org/10.1002/joc.2106

Sailor, D.J., Lu, L., 2004. A top–down methodology for developing diurnal and seasonal anthropogenic heating profiles for urban areas. Atmos. Environ. 38, 2737-2748. https://doi.org/10.1016/j.atmosenv.2004.01.034

Sun, R., Wang, Y., Chen, L., 2018. A distributed model for quantifying temporal-spatial patterns of anthropogenic heat based on energy consumption. J. Clean Prod. 170, 601-609. https://doi.org/10.1016/j.jclepro.2017.09.153

Tewari, M., Chen, F., Wang, W., Dudhia, J., LeMone, M., Mitchell, K., Ek, M., Gayno, G., Wegiel, J., Cuenca, R., 2004. Implementation and verification of the unified NOAH land surface model in the WRF model. 20th conference on weather analysis and forecasting/16th conference on numerical weather prediction. 1115, 2165-2170.

Vahmani, P., Luo, X., Jones, A., Hong, T., 2022. Anthropogenic heating of the urban environment: An investigation of feedback dynamics between urban micro-climate and decomposed anthropogenic heating from buildings. Build. Environ. 213, 108841. https://doi.org/10.1016/j.buildenv.2022.108841

Vargo, L.J., Anderson, B.M., Dadic, R., Horgan, H.J., Mackintosh, A.N., King, A.D., Lorrey, A.M., 2020. Anthropogenic warming forces extreme annual glacier mass loss. Nat. Clim. Change 10, 856-+. https://doi.org/10.1038/s41558-020-0849-2

Varquez, A.C.G., Kiyomoto, S., Khanh, D.N., Kanda, M., 2021. Global 1-km present and future hourly anthropogenic heat flux. Sci. Data 8, 1-14. https://doi.org/10.1038/s41597-021-00850-w

Wang, J., Miao, S.G., Doan, Q.V., Chen, F., Abolafia-Rosenzweig, R., Yang, L., Zhang, G.W., Zhang, Y.Z., Dou, J.J., Xu, Y.P., 2023. Quantifying the Impacts of High-Resolution Urban Information on the Urban Thermal Environment. J. Geophys. Res.-Atmos. 128, e2022JD038048. https://doi.org/10.1029/2022jd038048

Wang, K., Aktas, Y.D., Malki-Epshtein, L., Wu, D., Bin Abdullah, M.F.A., 2022a. Mapping the city scale anthropogenic heat emissions from buildings in Kuala Lumpur through a top-down and a bottom-up approach. Sust. Cities Soc. 76, 103443.

https://doi.org/10.1016/j.scs.2021.103443

Wang, S., Hu, D., Yu, C., Wang, Y., Chen, S., 2022b. Global mapping of surface 500-m anthropogenic heat flux supported by multi-source data. Urban CLim. 43, 101175. https://doi.org/10.1016/j.uclim.2022.101175

Wang, S.S., Hu, D.Y., Chen, S.S., Yu, C., 2019. A Partition Modeling for Anthropogenic Heat Flux Mapping in China. Remote Sens. 11, 1132. https://doi.org/10.3390/rs11091132

Wang, S.S., Hu, D.Y., Yu, C., Wang, Y.C., Chen, S.S., 2022c. Global mapping of surface 500-m anthropogenic heat flux supported by multi-source data. Urban CLim. 43, 101175. https://doi.org/10.1016/j.uclim.2022.101175

Wang, Y.C., Hu, D.Y., Yu, C., Di, Y.F., Wang, S.S., Liu, M.Q., 2022d. Appraising regional anthropogenic heat flux using high spatial resolution NTL and POI data: A case study in the Beijing-Tianjin-Hebei region, China. Environ. Pollut. 292, 118359. https://doi.org/10.1016/j.envpol.2021.118359

Wolpert, D.H., 1992. Stacked generalization. Neural Networks 5, 241-259. https://doi.org/https://doi.org/10.1016/S0893-6080(05)80023-1

Wu, H.T., Huang, B., Zheng, Z.J., Sun, R.H., Hu, D.Y., Zeng, Y., 2023a. Urban anthropogenic heat index derived from satellite data. Int. J. Appl. Earth Obs. Geoinf. 118, 103261. https://doi.org/10.1016/j.jag.2023.103261

Wu, W.B., Ma, J., Banzhaf, E., Meadows, M.E., Yu, Z.W., Guo, F.X., Sengupta, D., Cai, X.X., Zhao, B., 2023b. A first Chinese building height estimate at 10 m resolution (CNBH-10 m) using multi-source earth observations and machine learning. Remote Sens. Environ. 291, 113578. https://doi.org/10.1016/j.rse.2023.113578

Xie, M., Liao, J., Wang, T., Zhu, K., Zhuang, B., Han, Y., Li, M., Li, S., 2016. Modeling of the anthropogenic heat flux and its effect on regional meteorology and air quality over the Yangtze River Delta region, China. Atmos. Chem. Phys. 16, 6071-6089.

Xu, D., Zhou, D., Wang, Y.P., Meng, X.Z., Gu, Z.L., Yang, Y.J., 2021. Temporal and spatial heterogeneity research of urban anthropogenic heat emissions based on multi-source spatial big data fusion for Xi'an, China. Energy Build. 240, 110884. https://doi.org/10.1016/j.enbuild.2021.110884

Yang, B., Liu, H., Kang, E.L., Hawthorne, T.L., Tong, S.T.Y., Shu, S., Xu, M., 2022. Traffic restrictions during the 2008 Olympic Games reduced urban heat intensity and extent in Beijing. Commun. Earth Environ. 3, 105. https://doi.org/10.1038/s43247-022-00427-4

Yang, B., Yang, X., Leung, L.R., Zhong, S., Qian, Y., Zhao, C., Chen, F., Zhang, Y., Qi, J., 2019. Modeling the Impacts of Urbanization on Summer Thermal Comfort: The Role of Urban Land Use and Anthropogenic Heat. J. Geophys. Res.-Atmos. 124, 6681-6697. https://doi.org/10.1029/2018jd029829

Yu, C., Hu, D.Y., Wang, S.S., Chen, S.S., Wang, Y.C., 2021a. Estimation of anthropogenic heat flux and its coupling analysis with urban building characteristics - A case study of typical cities in the Yangtze River Delta, China. Sci. Total Environ. 774, 145805. https://doi.org/10.1016/j.scitotenv.2021.145805

Yu, Z., Hu, L.Q., Sun, T., Albertson, J., Li, Q., 2021b. Impact of heat storage on remote-sensing based quantification of anthropogenic heat in urban environments. Remote Sens. Environ. 262, 112520. https://doi.org/10.1016/j.rse.2021.112520

Zhan, C., Xie, M., 2022. Land use and anthropogenic heat modulate ozone by meteorology: a perspective from the Yangtze River Delta region. Atmos. Chem. Phys. 22, 1351-1371. https://doi.org/10.5194/acp-22-1351-2022

Zhang, G., Luo, Y., Zhu, S., 2020. Estimation of the Spatio-Temporal Characteristics of Anthropogenic Heat Emission in the Qinhuai District of Nanjing Using the Inventory Survey Method. Asia-Pac. J. Atmos. Sci. 56, 367-380. https://doi.org/10.1007/s13143-019-00142-9

Zheng, Y., Weng, Q., 2018. High spatial- and temporal-resolution anthropogenic heat discharge estimation in Los Angeles County, California. J. Environ. Manage. 206, 1274-1286. https://doi.org/10.1016/j.jenvman.2017.07.047

Supplementary Material

Table S1. Details of the data used in the study.

Data	Source (link)	Original resolution	Time range
Energy consumption data; Socioeconomic data **(**GDP, vehicles, population, administrative area, electricity consumption, freight volume**)**	Statistical yearbooks published by China's provincial and city statistical bureaus (http://www.stats.gov.cn/)	Table data	2019 and monthly
Nighttime lighting	Earth Observation Group, Payne Institute for Public Policy, Colorado School of Mines (https://eogdata.mines.edu/products/vnl/)	463.83 m	Monthly in 2019
MOD11A1-LST/ LST-night	NASA LP DAAC at the USGS EROS Center (https://lpdaac.usgs.gov/products/mod11a1v006/)	1000 m	Daily in 2019
Temperature, Wind speed, humidity	Famine Early Warning Systems Network (FEWS NET) Land Data Assimilation System (https://disc.gsfc.nasa.gov/datasets/FLDAS_NOAH01_C_GL_M_001/summary)	11132 m	Monthly in 2019
MOD13Q1-NDVI	NASA LP DAAC at the USGS EROS Center (https://lpdaac.usgs.gov/products/mod13q1v006/)	250 m	16-Day data in 2019
NASA NASADEM Digital Elevation	NASADEM Merged DEM Global 1 arc second ((https://lpdaac.usgs.gov/products/nasadem_hgtv001/))	30m	2000
Road and rail data	OpenStreetMap (https://www.openstreetmap.org)	Vector data	2019
Points of Interest	AutoNavi map (Amap, https://lbs.amap.com)	Vector data	2019 and 2020
Population heat data in representative cities	Baidu Huiyan big data platform (https://huiyan.baidu.com)	Vector data	Hourly for a day in 2019 and 2022

Calculation of the weighted road density:

$$w_l = V_l / \sum_{l}^{m} V_l$$

$$Density_s = \frac{\sum_r^n w_l^r \times L_r}{A_s}$$

where w_l is the weight of the road level l, V_l is the road design traffic volume for level l roads, m is the number of road levels; $Density_s$ is the weighted road density within the search radius, L_r is the length of the road r within the search radius, A_s is the area within the search radius, n is the number of roads in the search radius.

Calculation of the weighted factory density:

$$w_c = E_c / \sum_{c}^{m} V_c$$

$$Density_s = \frac{\sum_i^n w_c^i}{A_s}$$

where w_c is the weight of the factory type c, E_c is the energy consumption of industry type c, m is the number of industry types; $Density_s$ is the weighted factory density within the search radius, A_s is the area within the search radius, n is the number of factories in the search radius.